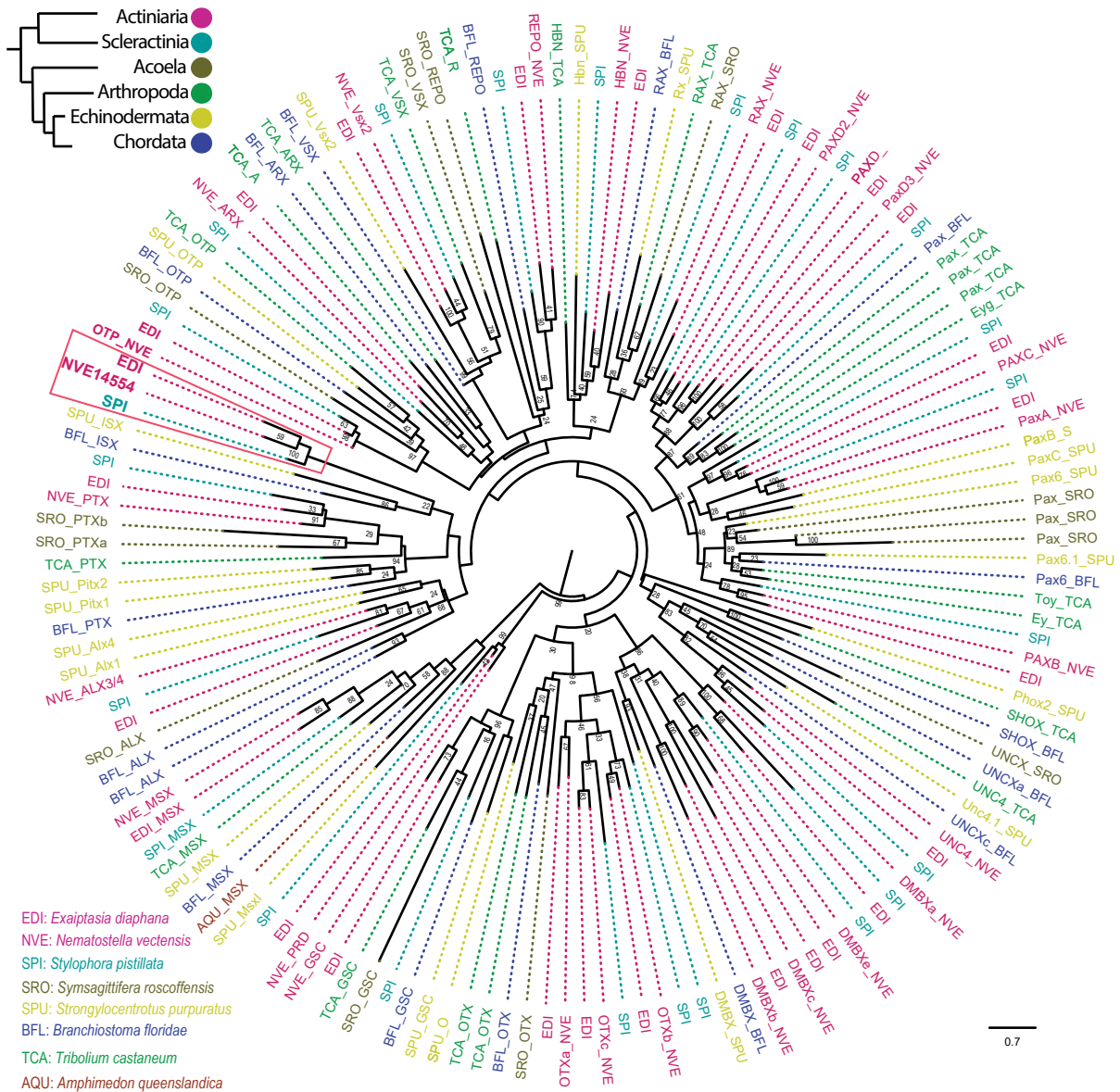
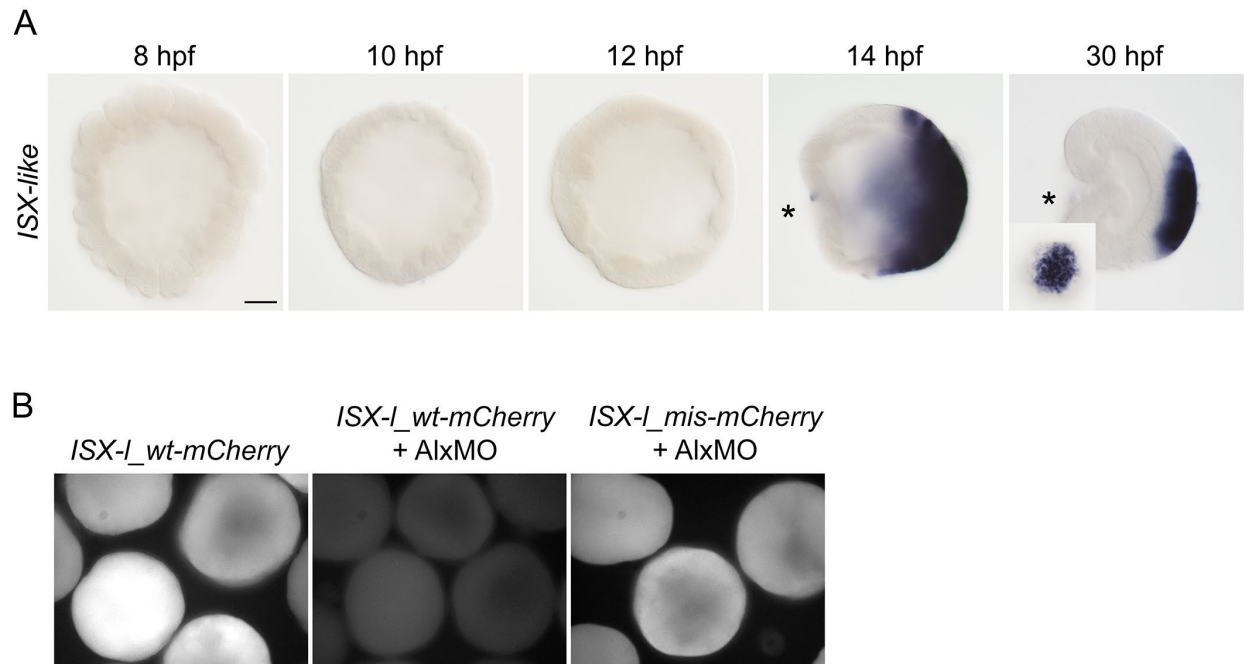


**Fig.S2. (A)** Sequence-similarity-based clustering of all *Nematostella* apical enriched GPCRs. Forty-six *Nematostella* GPCRs clustered with a large group of Rhodopsin and four clustered with Secretin. **(B)** Cluster map of the Rhodopsin cluster presented in A.



**Fig. S3. Maximum likelihood phylogenetic tree of PRD class homeobox of selected animals.**

The homeobox sequences of a representative selection of Cnidarians and bilaterian lineages (**Supplementary Table 1**) were aligned with MUSCLE algorithm [77] in the SeaView program [78]. The SMS: Smart Model Selection in PhyML [79] was used to determine the best-fitting model for the Phylogenetic reconstruction VT model (+G+F). The maximum-likelihood (ML) phylogenetic trees were constructed using PhyML v3.0 with 100 bootstrap [76]. Only bootstrap values of at least 20 at nodes are shown. The MSX family of ANTP class homeobox was used as an outgroup.



**Fig. S4. RNAi and morpholino efficiency.** (A) Early expression of ISX-like in *Nematostella* embryos. Inset on the 30 hpf gastrula image shows the aboral view. (B) Translation of the *mCherry* mRNA carrying the wild type recognition site of the ISX-like MO fused to it is efficiently suppressed by co-injecting ISX-like MO. In contrast, *mCherry* mRNA carrying the recognition site of the ISX-like MO with five introduced mismatches is efficiently translated in the presence of ISX-like MO. Lateral and aboral views, on lateral views, asterisk denotes the oral end. Scale bars 50  $\mu$ m.

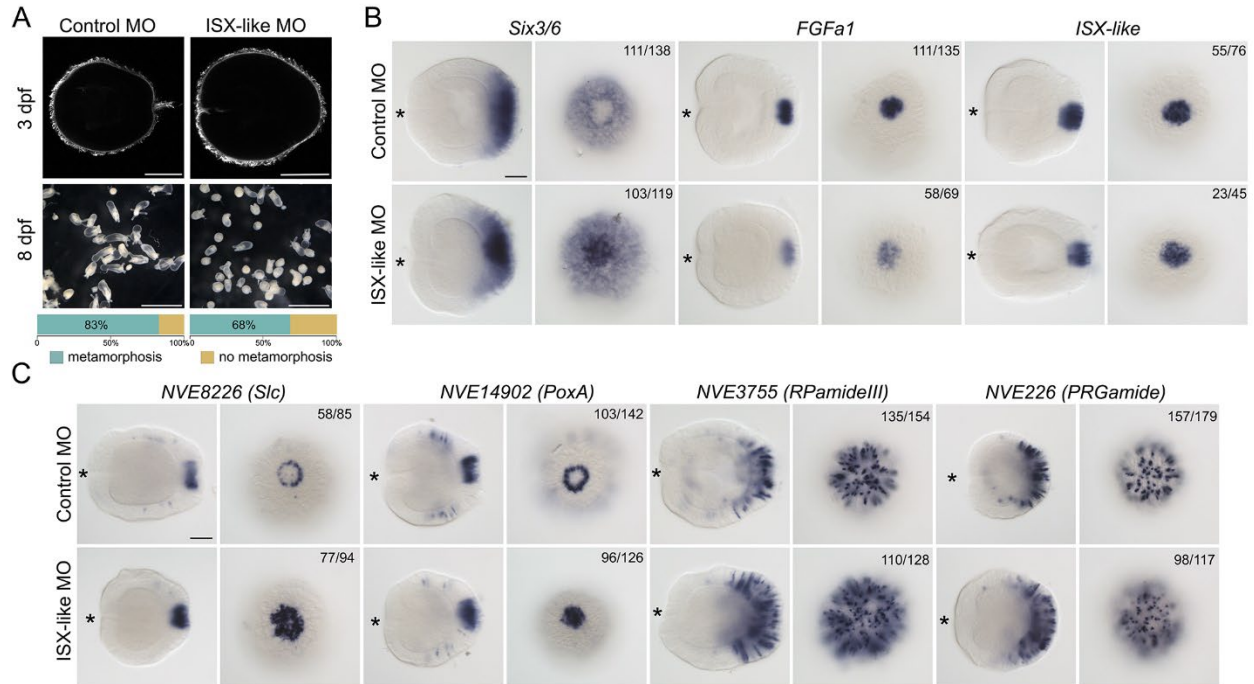


**Fig. S5. Effect of the morpholino-mediated knockdown of *ISX-like* phenocopies *ISX-like* RNAi.**

(A) Morpholino knockdown of *ISX-like* leads to a loss of the apical tuft (anti-acetylated tubulin staining, top row) and a mild reduction in the metamorphosis rate. (B) In *ISX-like* morphants, *Six3/6* expression expands into the apical domain, however, *FGFa1* and *ISX-like* are not strongly affected. (C) In *ISX-like* morphants, the expression of the ring genes extends into the pot domain, but the expression of the aborally enriched *PRGamide* (*NVE226*), and *RPamide III* (*NVE3775*) does not appear to be strongly affected. Lateral and aboral views, on lateral views, asterisk denotes the oral end. Scale bars on (A) 100  $\mu$ m, on (B) and (C) 50  $\mu$ m.



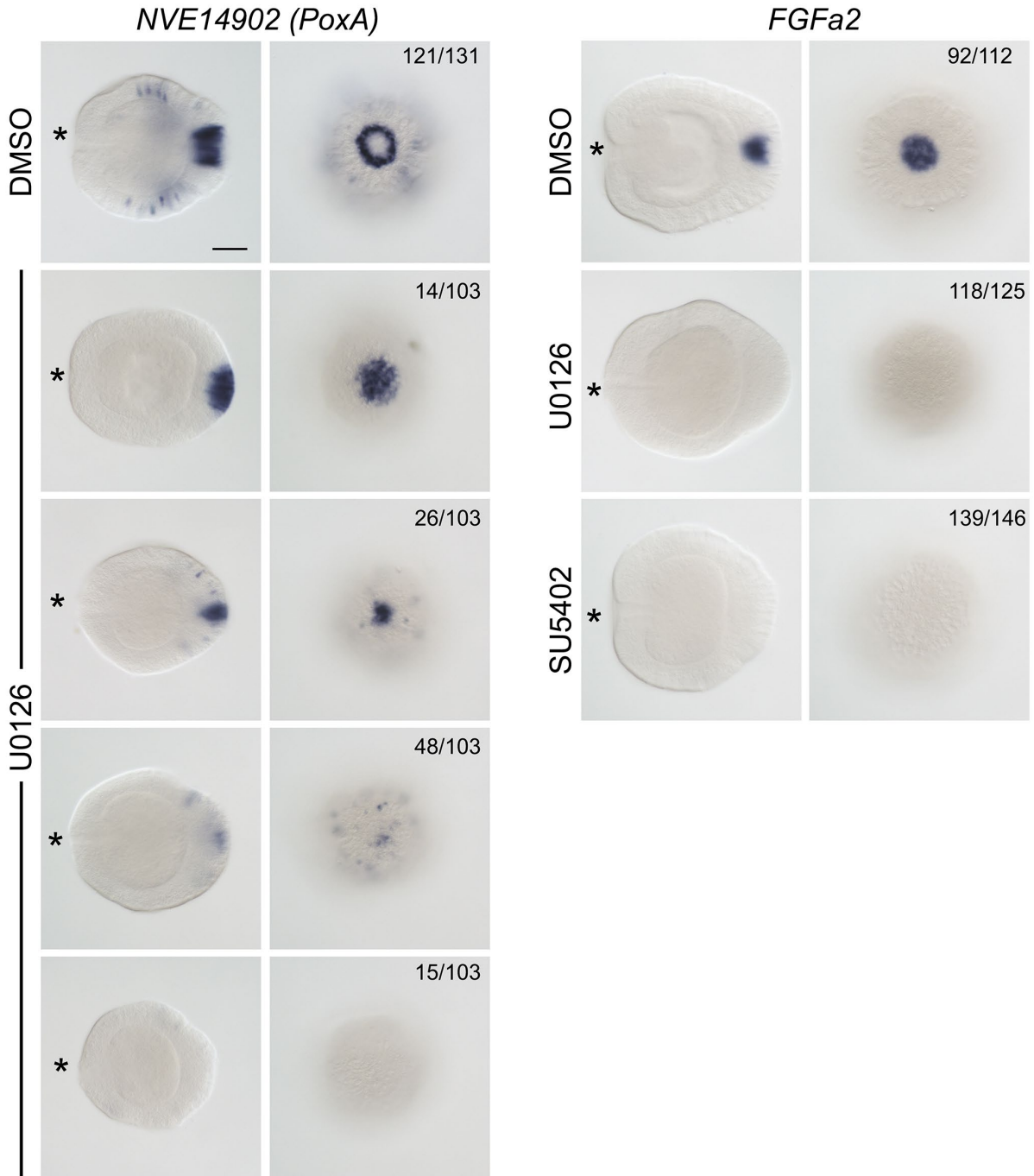
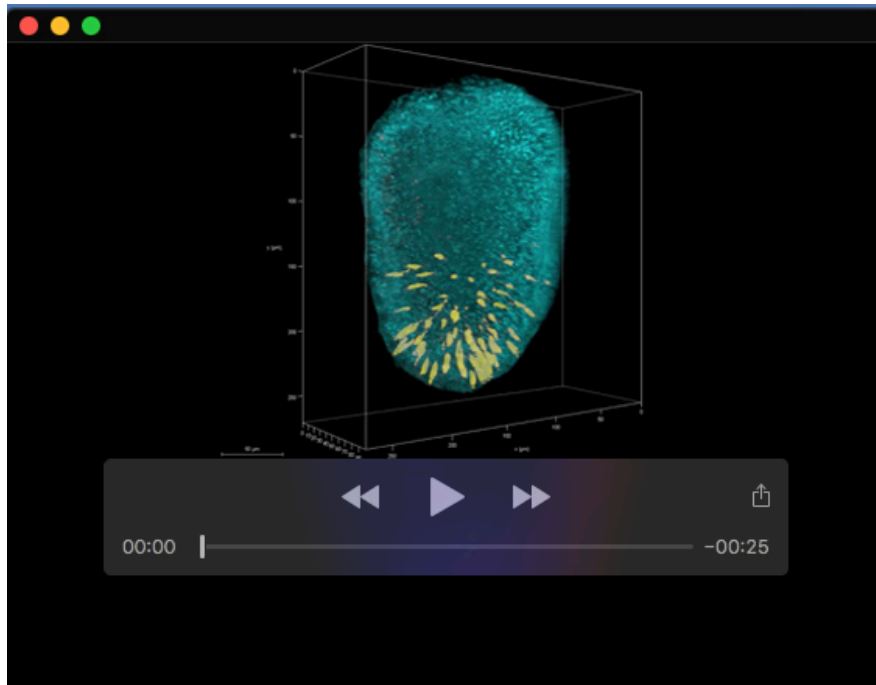


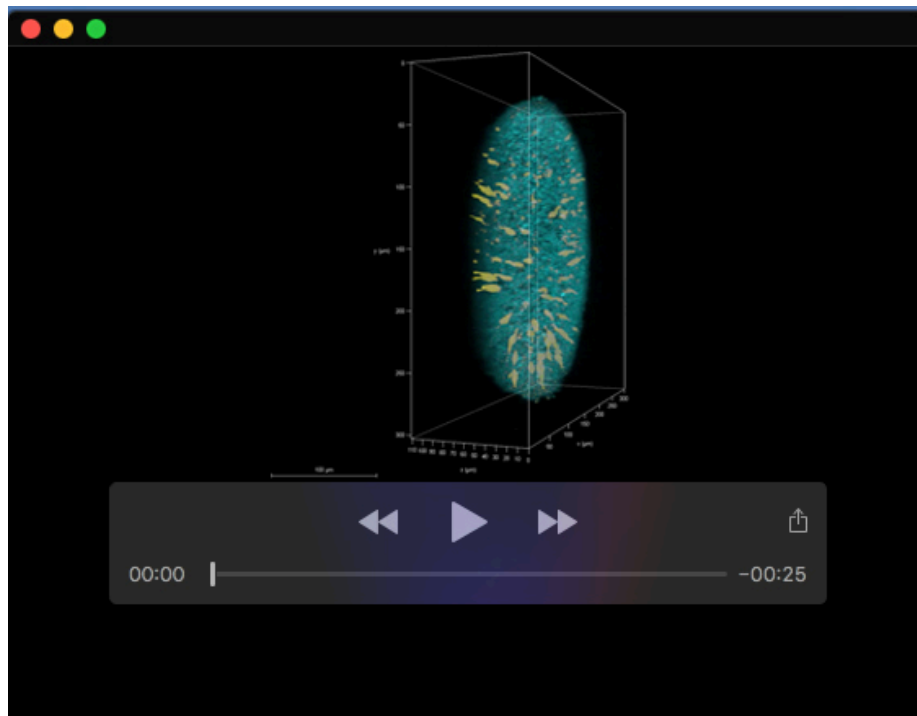
**Fig. S6. Variability of the effect of the U0126 treatment on NVE14902 expression and the effect of U0126 and SU5402 on FGFa2 expression.** Scale bar 50  $\mu\text{m}$ .

**Table S1.** Data relevant to figures 2, 3, 4, S1, S2 and S3.

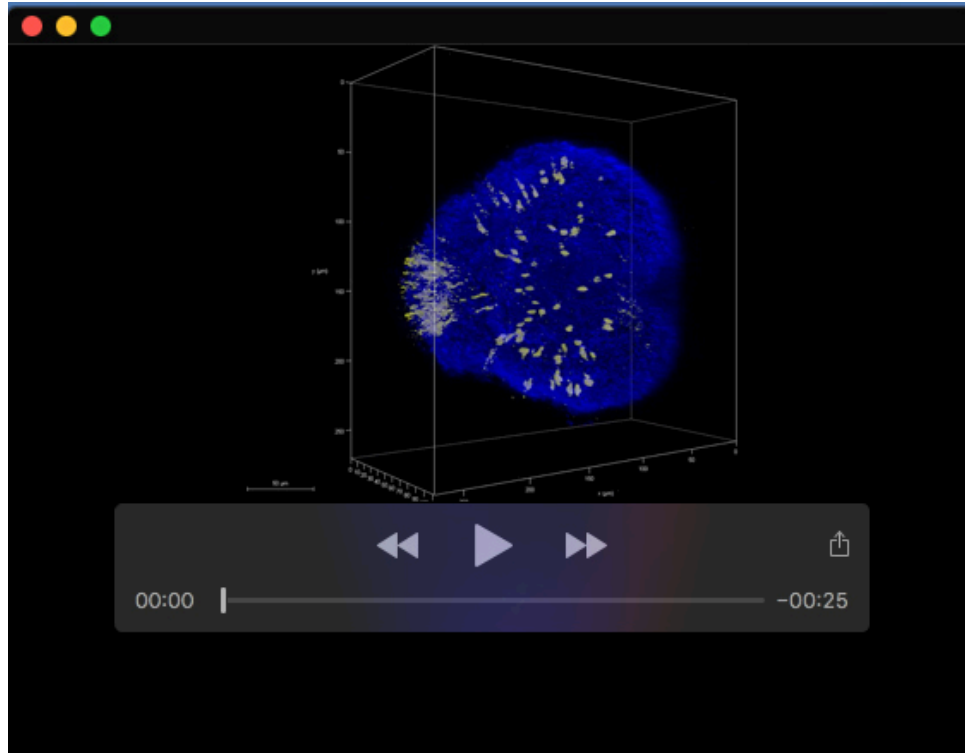
[Click here to download Table S1](#)



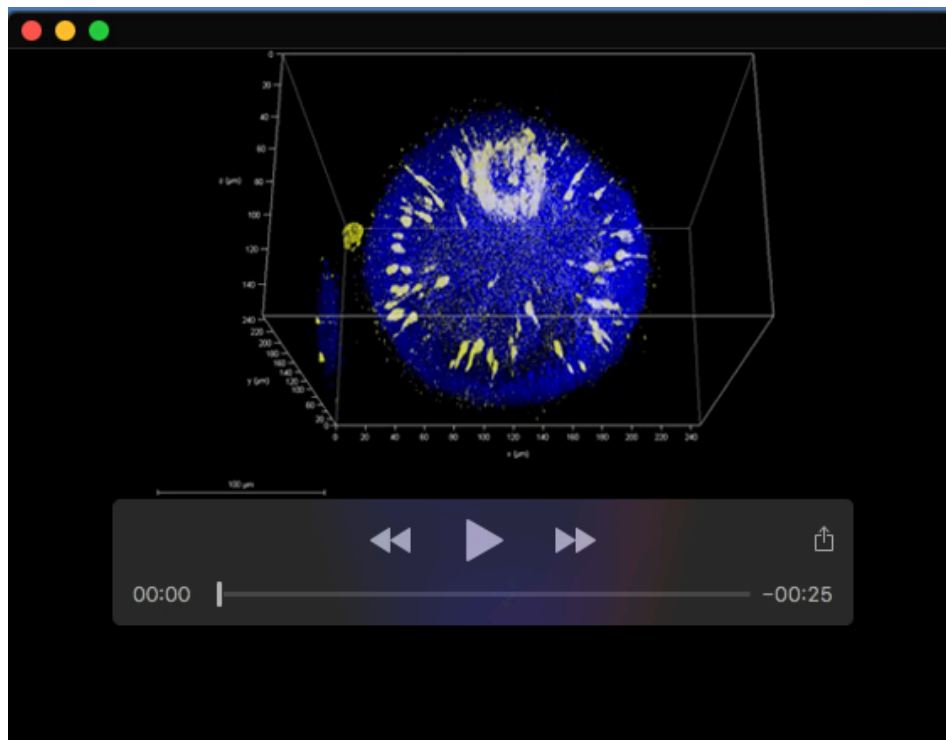
**Movie 1.** 3D view of fluorescence in situ hybridisation for gland/secretory cells type 1, related to Figure 5B&C. gland/secretory cells type 1 marker NVE22589 (yellow) and DAPI in cyan.



**Movie 2.** 3D view of fluorescence in situ hybridisation for gland/secretory cells type 3, related to Figure 5F. Gland/secretory cells type 3 marker NVE23674 (yellow) and DAPI in cyan.

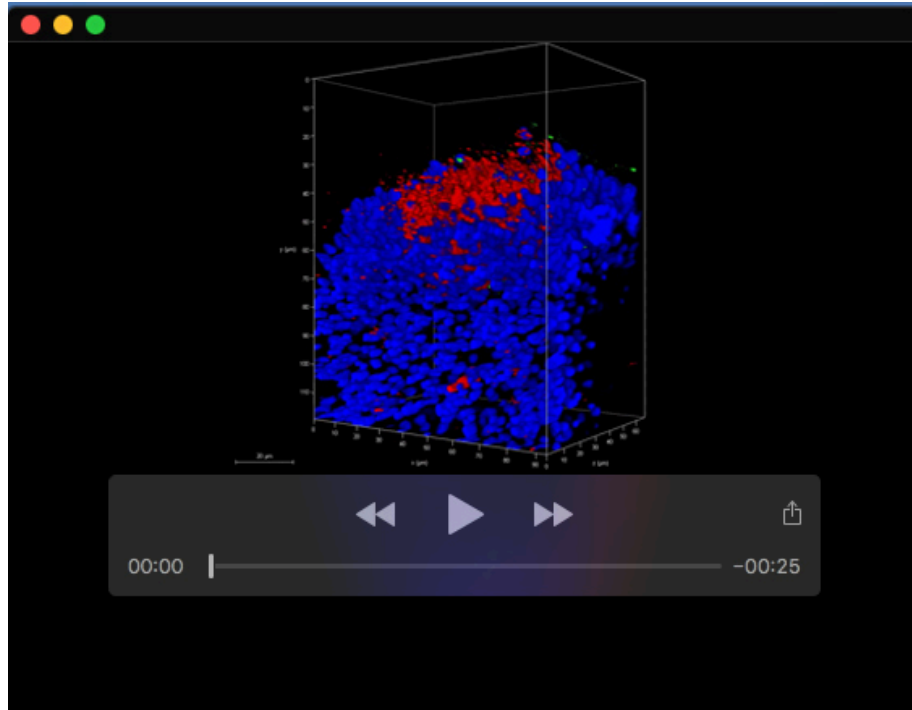


**Movie 3.** 3D view of fluorescence in situ hybridisation for larval-specific neuron gene, related to Figure 6A. *NVE8226* mRNA probe (yellow) and DAPI in Blue.

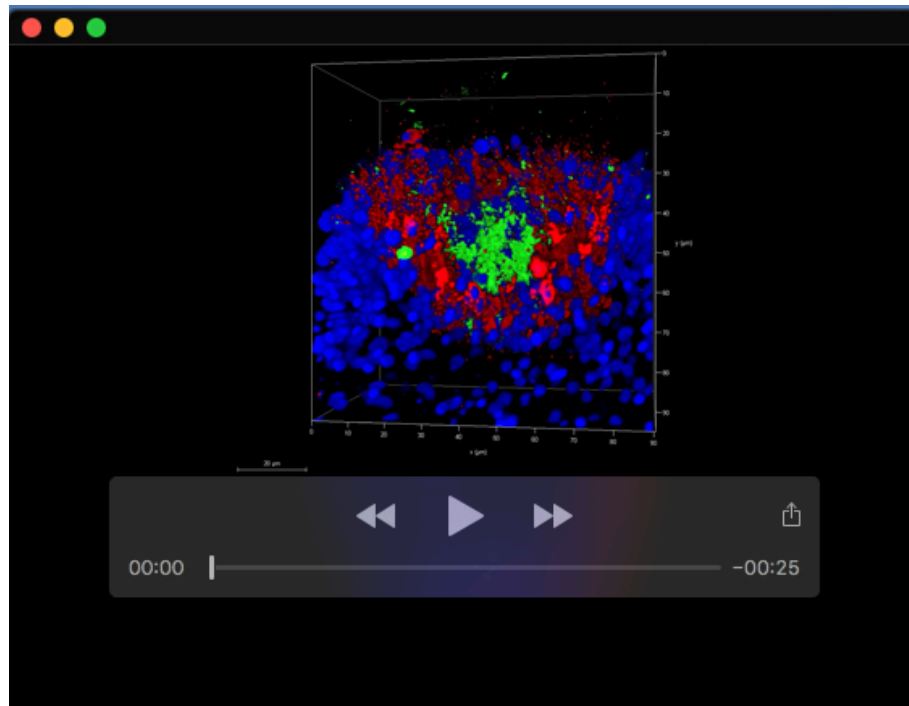


**Movie 4.** 3D view of fluorescence in situ hybridisation for larval-specific neuron gene, related to Figure 6E. *NVE14902* mRNA probe (yellow) and DAPI in Blue.





**Movie 5.** 3D view of Double fluorescence in situ hybridisation for spot probe *NVE14554* (green) and rind *NVE8226* (red) mRNA probes, related to Figure 6L. DAPI in Blue.



**Movie 6.** 3D view of Double fluorescence in situ hybridisation for spot probe *NVE14554* (green) and rind *NVE14902* (red) mRNA probes, related to Figure 6M. DAPI in Blue.